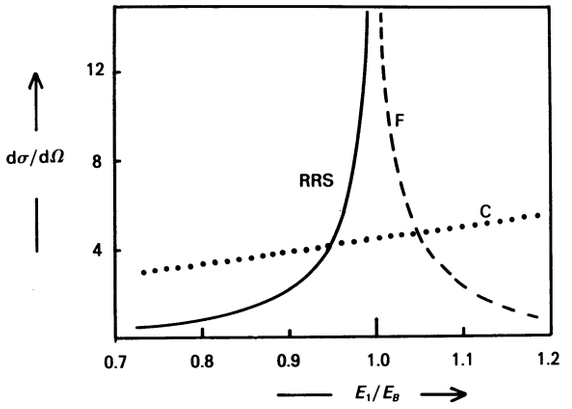

Fig. 7.4.3.3. The cross section for resonant Raman scattering (RRS) and fluorescence (F) as a function of the ratio of the incident energy, E, and the K-binding energy, E_B. The units of $d\sigma/d\Omega$ are $(e^2/mc^2)^2$ and the data are taken from Bannett & Freund (1975). For comparison, the intensity of Compton scattering (C) from copper through an angle of 30° is also shown [data taken from Hubbell *et al*. (1975)].

scattering in the elastic spectrum. It is important because, as the resonance condition is approached, the intensity will exceed that due to Compton scattering and therefore play havoc with any corrections to total intensities based solely on the latter.

Although systematic tabulations of resonance Raman scattering do not exist, Fig. 7.4.3.3, which is based on the calculations of Bannett & Freund (1975), shows how the intensity of RRS clearly exceeds that of the Compton scattering for incident energies just below the absorption edge. However, since the problems posed by anomalous scattering and X-ray fluorescence are generally appreciated, the energy range $0.9 < E_1/E_B < 1.1$ is wisely avoided by crystallographers intent upon absolute intensity measurements.

7.4.3.5. *Magnetic scattering*

Finally, and for completeness, it should be noted that the intensity of Compton scattering from a magnetic material with a net spin moment will, in principle, differ from that from a non-magnetic material. For unpolarized radiation, the effects are only discernible at photon energies greatly in excess of the electron rest mass energy, $mc^2 = 511\,\text{keV}$, but for circularly polarized radiation effects at the 1% level can be found in Compton scattering experiments carried out at $E_1 \simeq 1/10\,mc^2$ on ferromagnets such as iron. See Lipps & Tolhoek (1954) for a comprehensive description of polarization phenomena in magnetic scattering and Lovesey (1993) for an account of the scattering theory.

7.4.4. White radiation and other sources of background (By P. Suortti)

7.4.4.1. *Introduction*

By definition, the background includes everything except the signal. In an X-ray diffraction measurement, the signal is the pattern of Bragg reflections. The profiles of the reflections should be determined by the structure of the sample, and so the broadening due to the instrument should be considered as background. In the ideal angle-dispersive experiment, a well collimated beam of X-rays having a well defined energy (and a polarization, perhaps) falls on the sample, and only the radiation scattered by the sample is detected. Furthermore, the detector should be able to resolve all the components of scattering by energy, so that each scattering process could be studied separately. It is obvious that only after this kind of analysis are the Bragg reflections (plus the possible disorder scattering) unequivocally separated from the background arising from other processes. In most cases, however, this analysis is not feasible, and the reflections are separated by using certain assumptions concerning their profile, and the success of this procedure depends on the peak-to-background ratio.

The ideal situation described above is all too often not encountered, and experimenters are satisfied with too low a level of resolution. The aim of the present article is to point out the sources of the unwanted and unresolved components of the registered radiation and to suggest how these may be eliminated or resolved, so that the quality of the diffraction pattern is as high as possible. The article can cover only a few of the possible experimental situations, and only the 'almost ideal' angle-dispersive instrument is considered. It is assumed that the beam incident on the sample is monochromatized by reflection from a crystal and that the scattered radiation is registered by a low-noise quantum detector, which is the standard arrangement for modern diffractometers. Filtered radiation and photographic recording are used in certain applications, but these are excluded from the following discussion. The wavelength-dispersive or Laue methods are becoming popular at the synchrotron-radiation laboratories, and a short comment on these techniques will be included. Other sections of this volume deal with the components of scattering that are present even in the ideal experiment: thermal diffuse scattering (TDS), Compton and plasmon scattering, fluorescence and resonant Raman scattering, multiple scattering (coherent and incoherent), and disorder scattering.

The rest of the background may be termed 'parasitic' scattering, and it arises from three sources:

(1) impurities of the incident beam;
(2) impurities of the sample;
(3) surroundings of the sample.

Parasitic scattering is occasionally mentioned in the literature, but it has hardly ever been the subject of a detailed study. Therefore, the present article will discuss the general principles of the minimization of the background and then illustrate these ideas with examples. Most of the discussion will be directed to the first of the three sources of parasitic scattering, because the other two depend on the details of the experiment.

7.4.4.2. *Incident beam and sample*

An ideal diffraction experiment should be viewed as an X-ray optical system where all the parts are properly matched for the desired resolution and efficiency. The impurities of the incident beam are the wavelengths and divergent rays that do not contribute to the signal but scatter from the sample through the various processes mentioned above. The propagation of the X-ray beam through the instrument is perhaps best illustrated by the so-called phase-space analysis. The three-dimensional version, which will be used in the following, was introduced by Matsushita & Kaminaga (1980) and was elaborated further by Matsushita & Hashizume (1983). The width, divergence and wavelength range of the beam are given as a contour diagram, which originates in the X-ray source, and is modified by slits, monochromator, sample, and the detection system. The actual five-dimensional diagram is usually given as three-dimensional projections on the plane of diffraction and on the plane perpendicular to it and the beam axis, and in most cases the first projection is sufficient for an adequate description of the geometry of the experiment.

The limitations of the actual experiments are best studied through a comparison with the ideal situation. A close approximation to the ideal experimental arrangement is shown in Fig. 7.4.4.1 as a series of phase-space diagrams. The characteristic radiation from a conventional X-ray tube is almost uniformly distributed over the solid angle of 2π, and the relative width of the $K\alpha_1$ or $K\alpha_2$ emission line is typically $\Delta\lambda/\lambda = 5 \times 10^{-4}$. The acceptance and emittance windows of a flat perfect crystal are given in Fig. 7.4.4.1(*b*). The angular acceptance of the crystal (Darwin width) is typically less than 10^{-4} rad, and, if the width of the slit s or that of the crystal is small enough, none of the $K\alpha_2$ distribution falls within the window. Therefore, it is sufficient to study the size and divergence distributions of the beam in the $\lambda(K\alpha_1)$ plane only, as shown in Fig. 7.4.4.1(*c*). The beam transmitted by the flat monochromator and a slit is shown as the hatched area, and the part reflected by a small crystal by the cross-hatched area. The reflectivity curve of the crystal is probed when the crystal is rotated. In this schematic case, almost 100% of the beam contributes to the signal. The typical reflection profile shown in Fig. 7.4.4.2 reveals the details of the crystallite distribution of the sample (Suortti, 1985). The broken curve shows the calculated profile of the same reflection if the incident beam from a mosaic crystal monochromator had been used (see below).

The window of acceptance of a flat mosaic crystal is determined by the width of the mosaic distribution, which may be 100 times larger than the Darwin width of the reflection in

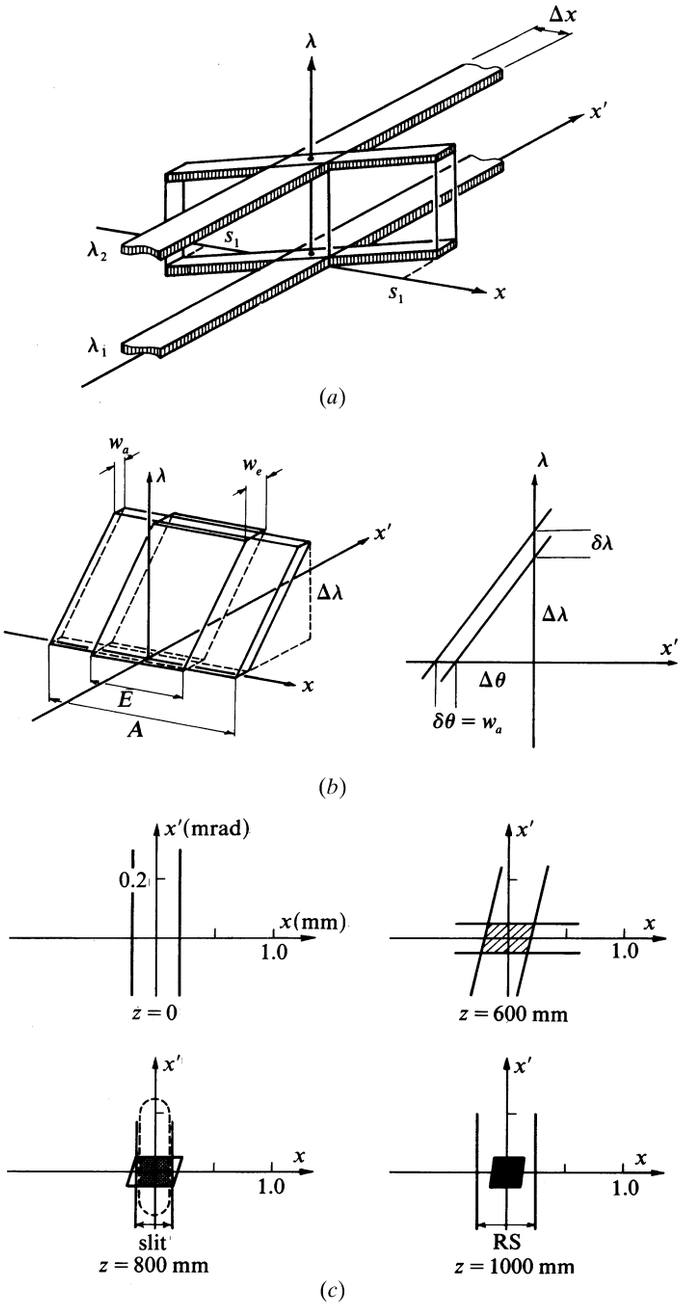

Fig. 7.4.4.1. Equatorial phase-space diagrams for a conventional X-ray source and parallel-beam geometry; x is the size and $x' = \mathrm{d}x/\mathrm{d}z$ the divergence of the X-rays. (*a*) Radiation distributions for two wavelengths, λ_1 and λ_2, at the source of width Δx, and downstream at a slit of width $\pm s_1$. (*b*) Acceptance and emittance windows of a flat perfect crystal, where the phase-space volume remains constant, $Aw_a\Delta\lambda = Ew_e\Delta\lambda$, and the (x', λ) section shows the reflection of a polychromatic beam (Laue diffraction). (*c*) Distributions for one wavelength at the source, flat perfect-crystal monochromator, sample (marked with the broken line), and the receiving slit (RS); z is the distance from the source.

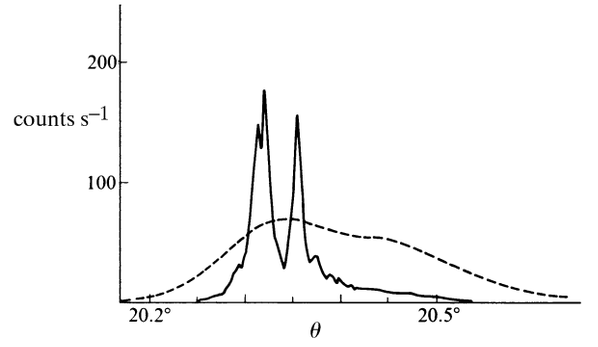

Fig. 7.4.4.2. Reflection 400 of LiH measured with a parallel beam of Mo $K\alpha_1$ radiation (solid curve). The broken curve shows the reflection as convoluted by a Gaussian instrumention function of $2\sigma = 0.1^\circ$ and $\theta(\alpha_2) - \theta(\alpha_1) = 0.13^\circ$, which values are comparable with those in Fig. 7.4.4.4.

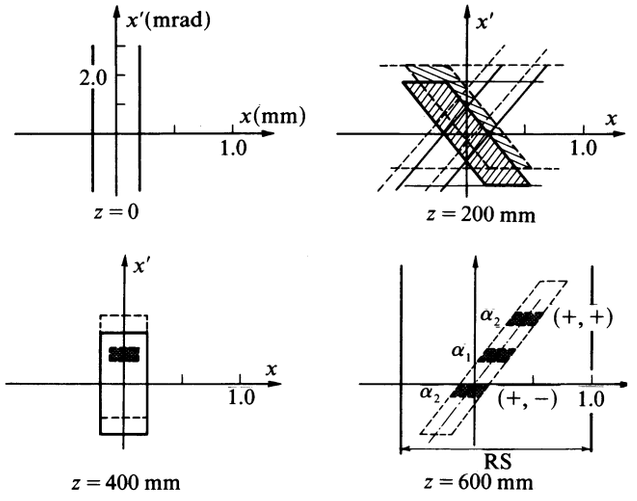

Fig. 7.4.4.3. Equatorial phase-space diagrams for two wavelengths, λ_1 (solid lines) and λ_2 (broken lines), projected on the plane $\lambda = \lambda_1$. The monochromator at $z = 200$ mm is a flat mosaic crystal, and a small sample is located at $z = 400$ mm, as shown by the shaded area. The reflected beams at the receiving slit are shown for the $(+, +)$ and $(+, -)$ configurations of the monochromator and the sample.

question. This means that a convergent beam is reflected in the same way as from a bent perfect crystal in Johann or Johansson geometry. Usually, the window is wide enough to transmit an energy band that includes both $K\alpha_1$ and $K\alpha_2$ components of the incident beam. The distributions of these components are projected on the (x, x', λ_1) plane in Fig. 7.4.4.3. The sample is placed in the (para)focus of the beam, and often the divergence of the beam is much larger than the width of the rocking curve of the sample crystal. This means that at any given time the signal comes from a small part of the beam, but the whole beam contributes to the background. The profile of the reflection is a convolution of the actual rocking curve with the divergence and wavelength distributions of the beam. The calculated profile in Fig. 7.4.4.2 demonstrates that in a typical case the profile is determined by the instrument, and the peak-to-background ratio is much worse than with a perfect-crystal monochromator.

An alternative arrangement, which has become quite popular in recent years, is one where the plane of diffraction at the monochromator is perpendicular to that at the sample. The beam is limited by slits only in the latter plane, and the wavelength varies in the perpendicular plane. An example of rocking curves measured by this kind of diffractometer is given in Fig. 7.4.4.4. The $K\alpha_1$ and $K\alpha_2$ components are seen separately plus a long tail due to continuum radiation, and the profile is that of the divergence of the beam.

In the Laue method, a well collimated beam of white radiation is reflected by a stationary crystal. The wavelength band reflected by a perfect crystal is indicated in Fig. 7.4.4.1(*b*). The mosaic blocks select a band of wavelengths from the incident beam and the wavelength deviation is related to the angular deviation by $\Delta\lambda/\lambda = \cot\theta\Delta\theta$. The angular resolution is determined by the divergences of the incident beam and the spatial resolution of the detector. The detector is not energy dispersive, so that the background arises from all scattering that reaches the detector. An estimate of the background level involves integrations over the incident spectrum at a fixed scattering angle, weighted by the cross sections of inelastic scattering and the attenuation factors. This calculation is very complicated, but at any rate the background level is far higher than that in a diffraction measurement with a monochromatic incident beam.

7.4.4.3. *Detecting system*

The detecting system is an integral part of the X-ray optics of a diffraction experiment, and it can be included in the phase-space diagrams. In single-crystal diffraction, the detecting system is usually a rectangular slit followed by a photon counter, and the slit is large enough to accept all the reflected beam. The slit can be stationary during the scan (ω scan) or follow the rotation of the sample ($\omega/2\theta$ scan). The included TDS depends on these choices, but otherwise the amount of background is proportional to the area of the receiving slit. It is obvious from a comparison between Fig. 7.4.4.1 and Fig. 7.4.4.3 that a much smaller receiving slit is sufficient in the parallel-beam geometry than in the conventional divergent-beam geometry. Mathieson (1985) has given a thorough analysis of various monochromator–sample–detector combinations and has suggested the use of a two-dimensional $\omega/2\theta$ scan with a narrow receiving slit. This provides a deconvolution of the reflection profile measured with a divergent beam, but the same result with better intensity and resolution is obtained by the parallel-beam techniques.

The above discussion has concentrated on improving the signal-to-background ratio by optimization of the diffraction geometry. This ratio can be improved substantially by an energy-dispersive detector, but, on the other hand, all detectors have some noise, which increases the background. There have been marked developments in recent years, and traditional technology has been replaced by new constructions. Much of this work has been carried out in synchrotron-radiation laboratories (for

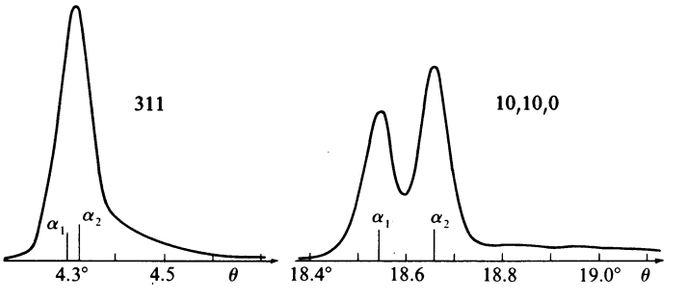

Fig. 7.4.4.4. Two reflections of beryllium acetate measured with Mo $K\alpha$. The graphite (002) monochromator reflects in the vertical plane, while the crystal reflects in the horizontal plane. The equatorial divergence of the beam is 0.8°, FWHM.

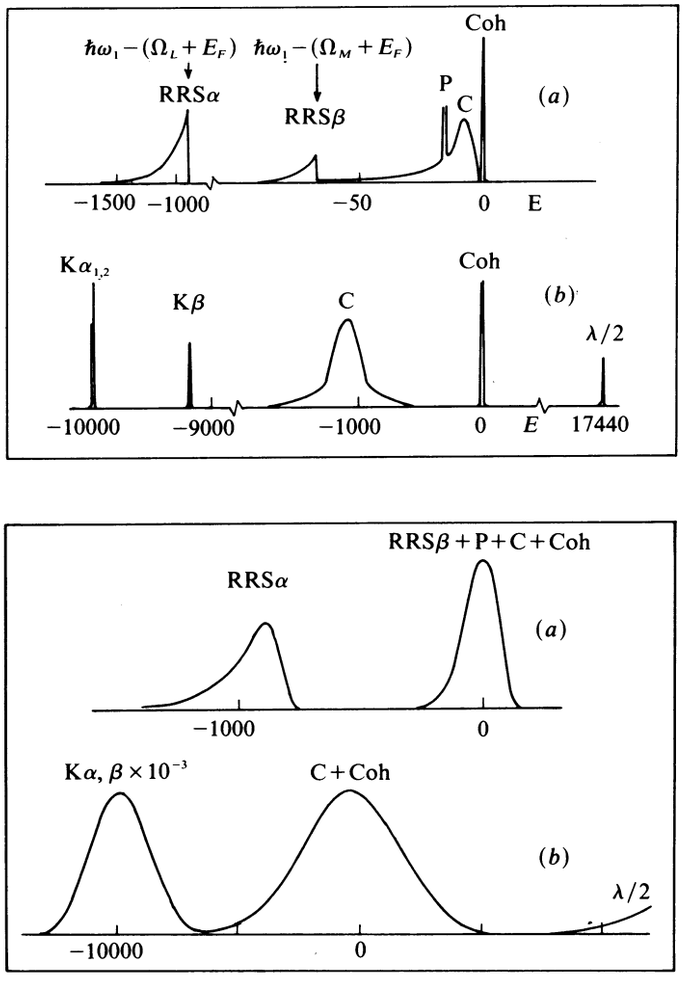

Fig. 7.4.4.5. Components of scattering at small scattering angles when the incident energy is just below the *K* absorption edge of the sample [upper part, (*a*)], and at large scattering angles when the incident energy is about twice the *K*-edge energy [upper part, (*b*)]. The abbreviations indicate resonant Raman scattering (RRS), plasmon (P) and Compton (C) scattering, coherent scattering (Coh) and sample fluorescence ($K\alpha$ and $K\beta$). The lower part shows these components as convoluted by the resolution function of the detector: (*a*) a SSD and (*b*) a scintillation counter (Suortti, 1980).

references